Vol 16 No 3, March 2007
1009-1963/2007/16(03)/0805-07

Chinese Physics

© 2007 Chin. Phys. Soc.
and IOP Publishing Ltd

Investigation on stability of directionally solidified CBr_4–C_2Cl_6 lamellar eutectic by using multiphase field simulation*

Zhu Yao-Chan(朱耀产)†, Wang Jin-Cheng(王锦程),
Yang Gen-Cang(杨根仓), and Zhao Da-Wen(赵达文)

State Key Laboratory of Solidification Processing, Northwestern Polytechnical University, Xi'an 710072, *China*

(Received 6 January 2006; revised manuscript received 19 December 2006)

With the multiphase field method, the stability of lamellar basic state is investigated during the directional solidification of eutectic alloy CBr_4–C_2Cl_6. A great number of lamellar patterns observed in experiments are simulated, and a stability diagram for lamellar pattern selections is presented. The simulated growth behaviours of these patterns are found to be qualitatively consistent with Karma *et al*'s numerical calculations and experimental results. The formation of the primary instability is attributed to the destabilization of solute boundary layer.

Keywords: multiphase field, directional solidification, morphological instability, stability diagram
PACC: 6480G, 7115Q, 8130F

1. Introduction

The steady-state growth of lamellar eutectics is well described by the Jackson–Hunt theory,[1] which indicates that a lamellar structure, called basic state, can exist in a limited continuous range of spacing, and the stability of the basic state beyond this range is also heuristically discussed. In 1981, Datye and Langer[2] predicted the period-doubling oscillatory ($2\lambda O$) mode of basic state analytically, and their prediction was numerically confirmed by Karma[3] in 1987, who discovered a tilt (T) mode moreover. Thereafter, the problem about the stability of lamellar basic state was well studied both experimentally and theoretically. By using the boundary integral approach, Karma and Sakissian[4] explored this problem in details in a quasistationary approximation of diffusion equation, and summarized their results of eutectic alloy CBr_4-C_2Cl_6 growth into a microstructure selection map (stability diagram). In 1996, these results were demonstrated experimentally by Ginibre *et al*,[5] and more other kinds of instability modes were discovered.

During the destabilization of lamellar basic state, catastrophic dynamic events often take place, such as the merging of two lamella and nucleation, and they can hardly be handled by the boundary integral approach, but easily and efficiently treated by using multiphase field method, which is mainly because the interfaces involved during eutectic growth are implicitly described. Consequently, both the advantage of multiphase field method over the numerical boundary integral approach, and the situation in which most of the multiphase field models of eutectic growth are only for eutectic composition[6−9] or several isolated compositions,[10] motivate us to systemically investigate the stability of basic state of eutectic alloy CBr_4-C_2Cl_6 in the whole composition range. In this paper, the multiphase field model in Ref.[10] is adopted. In order to compare simulations with the stability diagram by the boundary integral calculation[4] and the experiments,[5] the results by Kim *et al* [10] for eutectic compositions (dimensionless composition $\eta = 0.2$) and hypereutectic composition ($\eta = 0.5$) are repeated.

2. Model

During binary eutectic solidification, two solid phases (α and β) grow from liquid phase (L), leading to several bulk phases and interfaces involved. To distinguish them, three order parameters named phase fields are introduced, which are casually iden-

*Project supported by the National Natural Science Foundation of China (Grant No 50271057).
†E-mail: zhuyaocan1978@hotmail.com

tified with the fraction of phases. Each bulk phase is represented by phase field $\phi_i = 1$ in a distinct phase region of the phase space, and $\phi_i = 0$ otherwise. As a result, each interface is represented implicitly by the gradual variation of corresponding phase field, and at any point of phase space, the following constraint holds:

$$\sum_{i=1}^{3} \phi_i = 1. \tag{1}$$

The multiphase field model in Ref.[10] has an advantage over other multiphase models[6−9] that the chemical potential is continuous and equal inside interfaces. The phase field equation of this model could be expressed by using the interface field method[11] as

$$\frac{\partial \phi_i}{\partial t} = -\frac{2}{n}\sum_{j\neq i}^{3} s_{ij} M_{ij}\Big[\frac{\delta F}{\delta \phi_i} - \frac{\delta F}{\delta \phi_j}\Big] \tag{2}$$

with

$$\frac{\delta F}{\delta \phi_i} = \sum_{j\neq i}\Big[\frac{\varepsilon_{ij}^2}{2}\nabla^2\phi_j + \omega_{ij}\phi_j\Big] + f^i(c_i) - c_i f_c, \tag{3}$$

$$f^i(c_i) - c_i f_c = -\frac{RT_{\rm E}}{v_m}\Big(c_{\rm E} - \frac{T_{\rm E} - T}{m_i}\Big)(1 - k_i) - \frac{RT_{\rm E}}{v_m}c_i, \tag{4}$$

where

$f^i(c_i)$: free energy density of the ith phase with composition c_i;

ε_{ij}: gradient energy coefficient;

ω_{ij}: height of the double-well potential;

s_{ij}: variable correlated with the number of interfaces in a given domain;

M_{ij}: kinetic coefficient of phase field;

$c_{\rm E}$: eutectic composition;

$T_{\rm E}$: eutectic temperature;

K_i: equilibrium partition coefficient;

m_i: equilibrium liquidus slope.

The compositions of any coexisting phase are constrained by equal chemical potential condition

$$f^1_{c_1}(c_1) = f^2_{c_2}(c_2) = f^3_{c_3}(c_3) = f_c. \tag{5}$$

By a mixture rule, the average composition could be expressed as

$$c(x,t) = \sum_{i}^{3} \phi_i(x,t)c_i(c,t). \tag{6}$$

The mass conversation equation follows

$$\frac{\partial c}{\partial t} = \nabla \cdot D(\phi_3)\sum_{i=1}^{3}\phi_i \nabla c_i \tag{7}$$

with

$$D(\phi_3) = D_{\rm S}(\phi_3 < 0.1),\ D_{\rm L}(\phi_3 \geq 0.1), \tag{8}$$

where $D_{\rm S}$ and $D_{\rm L}$ are the solute diffusivities in solid and liquid phases respectively.

The multiphase field model is composed of phase field equation (2) and mass conversation equation (7). By mapping this model into a two-phase system, we can obtain the following relationships between material parameters and phase field parameters:[10]

$$2\xi = \pi\frac{\varepsilon_{i3}}{\sqrt{2\omega_{i3}}}, \tag{9}$$

$$\sigma_{i3} = \frac{\pi}{8}\varepsilon_{i3}\sqrt{2\omega_{i3}}, \tag{10}$$

$$\beta_{i3} = -\frac{v_m}{M_{i3}RT}\frac{m_i}{1-k_i}\frac{\sigma_{i3}}{\varepsilon_{i3}^2} + \frac{m_i(1-k_i)\varepsilon_{i3}}{\sqrt{2\omega_{i3}}}c^e_{3i}\zeta_{i3}, \tag{11}$$

where ξ is the interface width, ζ_{i3} is the constant related to the form of free energy density function $f^i(c_i)$, and β_{i3} is the kinetic coefficient which has a vanishing value in our simulation.

3. Computational method and parameters

To numerically study this multiphase model, the uniform square grid at a rectangle calculation domain $l_x \times l_z$ is introduced. l_z is evaluated by $4l_{\rm D}$ where $l_{\rm D}$ is the characteristic solute diffusion length given by $l_{\rm D} = 2D_{\rm L}/V$; l_x is related to the initial lamellar spacing and the number of lamellae. On each side of the domain in the z-direction, which is parallel to the thermal gradient direction, periodic boundary condition is imposed, while the no-flux boundary condition on the other two sides in the x-direction. Two couples of lamellae are fixed artificially at the bottom of the domain (x-direction). The noise to composition field is introduced in the solid/liquid interface, serving as a perturbation which is expressed as

$$c = c^0(1 + \vartheta\chi\phi_3), \tag{12}$$

where c and c^0 are the compositions with and without a perturbation, respectively. ϑ represents the strength of the noise, and χ is the random number ranging from 0 to 1.

Jackson and Hunt have concluded[1] that the basic patterns are stable over a limited range of lamellar spacing λ. It is well documented in Ref.[5] that the lower bound of this range is determined by a local, lamella-termination instability and the upper bound is

marked by the bifurcation toward an oscillatory state. In this paper, the growth behaviours of directionally solidified CBr_4–C_2Cl_6 lamellar eutectic are simulated as a function of initial lamellar spacing λ, the composition c at a given velocity V (2.0×10^{-6} m/s) and thermal gradient G (0.8×10^4 K/m). The material parameters of CBr_4–C_2Cl_6 measured in Ref.[12] are used and listed in Table 1. In all computations, $\xi = 0.7 \times 10^{-6}$ m is taken.

Table 1. Parameters of CBr_4–C_2Cl_6 used in the simulation.[12]

Parameter	Value		Parameter	Value	
c_E	0.118	mol%	T_E	357.6	K
K_α	0.75		K_β	1.5	
m_α	−82	K/mol	m_β	164	K/mol
D_L	0.5×10^{-9}	m^2/s	D_S	0.5×10^{-13}	m^2/s
σ_{13}	6.6×10^{-3}	J/m^2	σ_{23}	5.8×10^{-3}	J/m^2
σ_{12}	11.5×10^{-3}	J/m^2			

For convenience, one uses the dimensionless composition defined as

$$\eta = \frac{c - c_\alpha}{c_\beta - c_\alpha}, \tag{13}$$

where c_α and c_β are the compositions at the ends of eutectic plateau of phase diagram. And the dimensionless initial lamellar spacing is expressed as

$$\Lambda = \lambda/\lambda_{JH}, \tag{14}$$

where λ_{JH} is the Jackson–Hunt minimum-undercooling lamellar spacing.

4. Results and discussion

The simulations under different conditions are briefly discussed and the transition between different instabilities is pointed out; meanwhile, some patterns are compared with those observed in experiments which we can find from literature, and then special attention is paid to the stability diagram and the primary modes. In all of our simulations, the composition field is shown, and in each figure the white region is β phase, the black one α phase, and the grey one the liquid phase, in which the shade of grey shows the variation of composition.

4.1. Hypoeutectic composition ($\eta = 0.2$)

When the initial spacing is small, lower than λ_{JH}, the overstability occurs. As it becomes lower ($\Lambda = 0.79$), the perturbation of the solute field causes the difference between the velocities of lamellae, which results in the lamellar termination as shown in Fig.1(a). For a rather broad range of Λ that is above 1, the lamellae grow in the form of basic state. Figure 1(b) shows this state for $\Lambda = 1.5$. When Λ reaches 2.6, the period-doubling oscillatory mode ($2\lambda O$ mode) of the instability is formed as shown in Fig.1(c), in which one type of lamella follows a wavy trajectory, while the other keeps the reflection symmetric. This morphology is closely similar to the $2\lambda O$ mode observed in experiments[5] as shown in Fig.2.

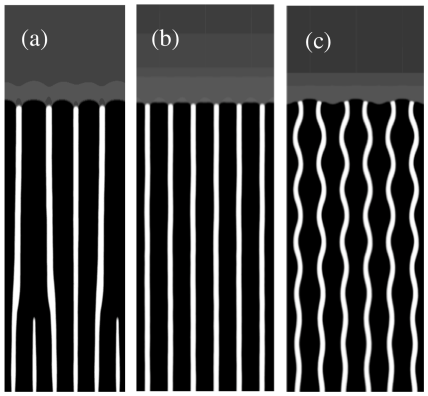


Fig.1. Simulated typical patterns of the hypoeutectic alloy with a composition of $\eta = 0.2$ at different initial spacings. (a) $\Lambda = 0.79$, lamellar termination; (b) $\Lambda = 1.5$, basic state; (c) $\Lambda = 2.6$, $2\lambda O$ mode.

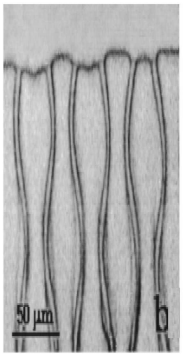


Fig.2. $2\lambda O$ mode of the hypoeutectic alloy observed in experiments.[5]

4.2. Eutectic composition ($\eta = 0.29$)

The typical patterns for the eutectic composition of $\eta = 0.29$ are shown in Fig.3 at different values of Λ: (a) $\Lambda = 0.75$ for lamellar termination, (b) $\Lambda = 2.3$ for basic state, (c) $\Lambda = 2.5$ for $1\lambda O$ mode and (d) $\Lambda = 2.7$ for $2\lambda O$ mode. In our simulations of nearing eutectic composition, besides the preceding $2\lambda O$ mode, the period-preserving oscillatory $1\lambda O$ mode also appears. In this $1\lambda O$ mode, half of the α (or β) lamellae with one lamellar spacing apart, oscillates in phase. When Λ is sufficiently higher than the value at which $1\lambda O$ mode occurs, the influence of volume fraction adjustment on two lamellar phases stands out further, and the $1\lambda O$ mode transforms rapidly into $2\lambda O$ mode. The mixture of these two modes could be observed in Fig.3(d). However, this state cannot be homogeneous and can exist only in a transition area. Note that the $1\lambda O$ mode and $2\lambda O$ mode in our simulations are λ- and c-dependent. It could be found that the morphologies obtained by simulation are analogous to the typical patterns observed in experiments[5,13] as shown in Fig.4.

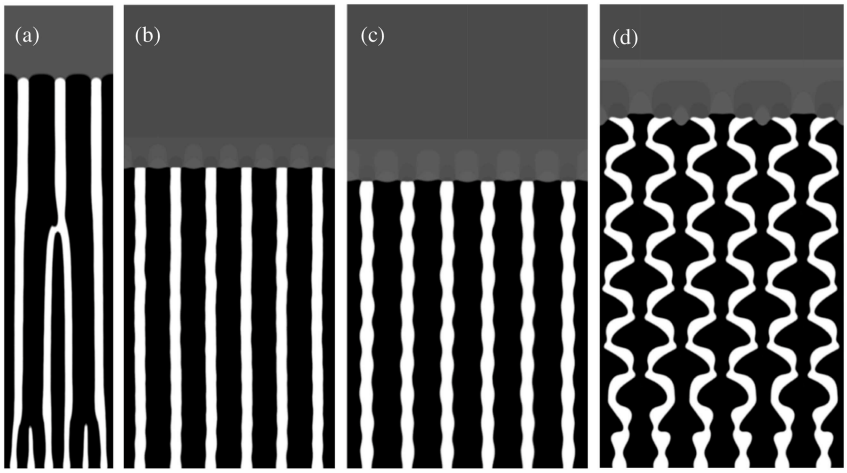


Fig.3. Simulated typical patterns of eutectic alloy with a composition of $\eta = 0.29$ at different initial spacings. (a) $\Lambda = 0.75$, lamellar termination; (b) $\Lambda = 2.3$, basic state; (c) $\Lambda = 2.5$, $1\lambda O$ mode; (d) $\Lambda = 2.7$, $2\lambda O$ mode.

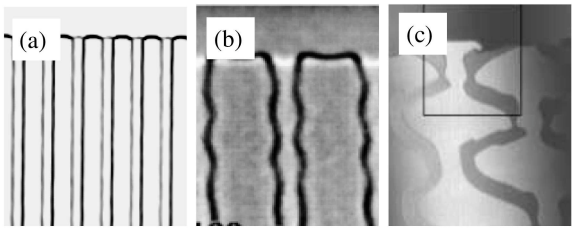


Fig.4. Typical patterns of eutectics observed in experiments. (a) basic state;[13] (b) $1\lambda O$ mode;[5] (c) $2\lambda O$ mode.[13]

4.3. Hypereutectic compositions ($\eta = 0.4$, $\eta = 0.5$ and $\eta = 0.6$)

Three hypereutectic compositions ($\eta = 0.4, 0.5, 0.6$) are purposefully chosen because composition range of hypereutectic is wider than that of hypoeutectic. Because of their similarity, only the results of $\eta = 0.5$ are shown in Fig.5 and some of the results can also be found in Ref.[10]. The typical patterns are (b) basic state at $\Lambda = 1.4$; (c) $2\lambda O$ mode at $\Lambda = 1.5$; (d) T-$2\lambda O$ mode at $\Lambda = 1.8$; (e) T mode at $\Lambda = 1.9$; (f) T-$1\lambda O$ mode at $\Lambda = 2.3$. Lamellar termination arises when $\Lambda = 0.8$ as shown in Fig.5(a). From Figs.1, 3 and 5, it could be found that the primary $2\lambda O$ instead of the primary $1\lambda O$ occurs at an off-eutectic composition. At the composition of $\eta = 0.5$, a new instability named 'tilt instability' (T mode), in which symmetric states disappear and lamellae grow at a tilt angle against the z-direction, occurs in the simulations. This tilt instability is the consequence of the long-wavelength modulations. Below the range of Λ in which T mode arises, the mixed instability T-2λO mode ($\Lambda = 1.8$) is simulated, which results from the instability of the basic states and T mode with re-

spect to the long-wavelength modulations; while above this range, the T mode transforms into the mixed instability T-1λO. The typical patterns observed in experiments[5] for hypereutectic alloy are shown in Fig.6, indicating the morphologies similar to simulation results.

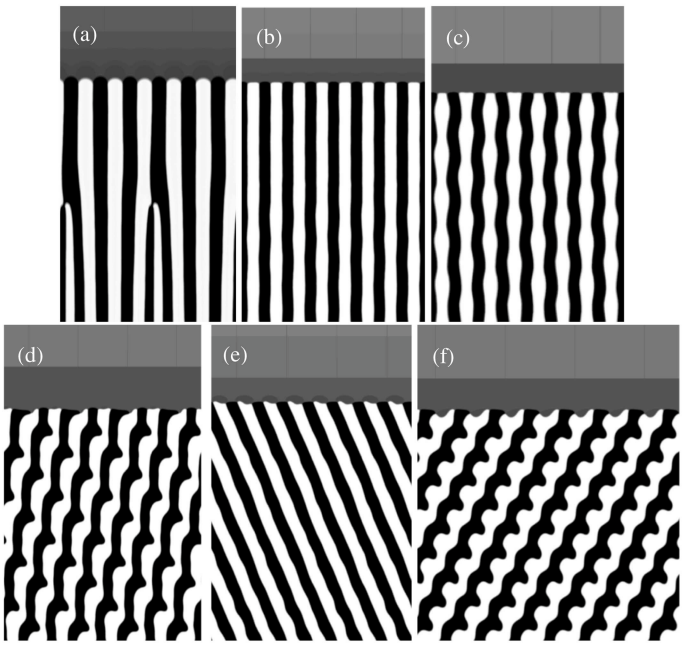


Fig.5. Simulated typical patterns of hypereutectic alloy with a composition of $\eta = 0.5$ at different initial spacings. (a) $\Lambda = 0.8$, lamellar termination; (b) $\Lambda = 1.4$, basic state; (c) $\Lambda = 1.5$, 2λO mode; (d) $\Lambda = 1.8$, T-2λO mode; (e) $\Lambda = 1.9$, T mode; (f) $\Lambda = 2.3$, T-1λO mode.

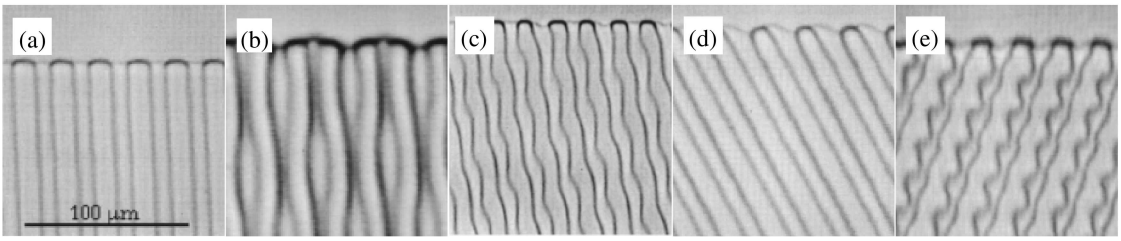


Fig.6. Typical patterns of hypereutectic alloys in experiments,[5] showing (a) basic state; (b) 2λO mode; (c) T-2λO mode; (d) T mode; (e) T-1λO mode.

4.4. Stability diagram

The simulations above can be summarized into a stability diagram as shown in Fig.7, in which the numerical calculations presented by Karma and Sakissian[4] are schematically plotted by lines. The solid line represents the stability boundary, and the dash dot line is for the lamellar termination threshold. Qualitatively, this diagram is in good agreement with the boundary integral calculations[4] and measurements[5] as shown in Fig.8, where the sequence of the onset of various instability modes of the basic state is considered. Moreover, it can be commonly found that the overstability occurs when Λ is less than 1, and its range decreases when η deviates from eutectic composition; At the exact or nearing eutectic composition, the 1λO mode arises and overtakes the preceding 2λO mode; On the side of hypereutectic composition, the value of Λ which is corresponding to instability mode, decreases rapidly as η increases. However, the corresponding value of Λ in our simulations is generally higher than those of boundary inte-

gral calculation[4] and experiments,[5] especially on the side of hypoeutectic composition as shown in Fig.7. As can be seen, this stability diagram is unsymmetrical, which results from the dissymmetry of the phase diagram. The remarkable difference in volume percentage between α phase and β phase causes a new lamella to nucleate readily in liquid in the front of the α phase during the solidification of hypoeutectic alloy, and after occurrence of $2\lambda O$ instability. That is why no T-$x\lambda O$ mode and T mode can be found except $2\lambda O$ mode. In other words, the formation of T mode could be partly ascribed to the dissymmetry of the phase diagram.[4]

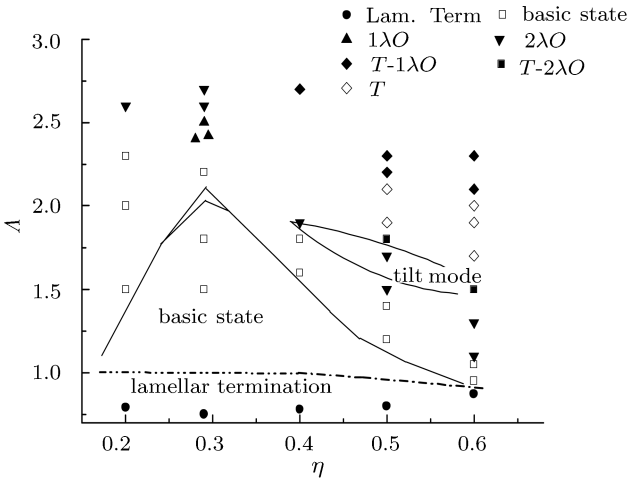


Fig.7. Stability diagram of directionally solidified CBr_4-C_2Cl_6 by multiphase field simulation. Lam. Term: lamellar termination. Curve: numerical calculation diagram by Karma and Sarkissian.[4]

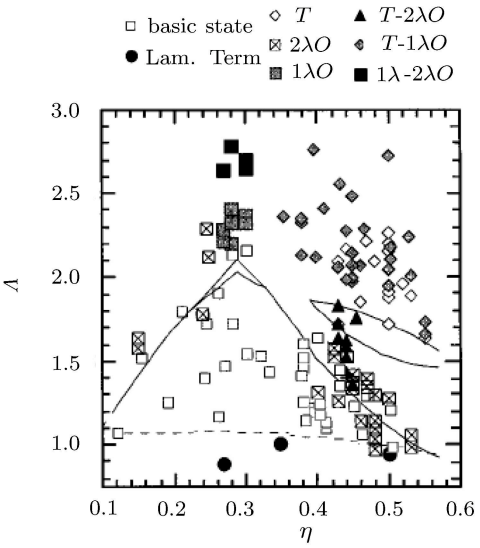


Fig.8. Stability diagram of directionally solidified CBr_4–C_2Cl_6 by experiments.[5] Curve: numerical calculation diagram by Karma and Sarkissian.[4]

Generally, the various instability modes of basic state result from the adjustment of volume faction and the solute redistribution.[14] However, through the whole range of composition, whichever instability mode is selected as the primary one cannot be determined according to this explanation. In our present study, the growth of lamella is diffusion-controlled, and it is supposed[3] that destabilization against the basic state originates from the Mullins–Sekerka instability[15] rooting in solute boundary layer. The solute distribution is[1]

$$c = c_{\mathrm{E}} + c_0 + B_0 \exp\Big(-\frac{V}{2D_{\mathrm{L}}}\Big) + \sum_{1}^{\infty} B_n \cos\Big(\frac{2n\pi x}{\lambda}\Big)\exp\Big(-\frac{2n\pi z}{\lambda}\Big), \tag{15}$$

which indicates that the diffusion field is composed of two parts: the lateral periodic diffusion field adjacent to the solid/liquid interface and the one-dimensional (1D) diffusion field which is dominated by the primary phase of off-eutectic alloy. Consequently, the Mullins–Sekerka instability wavelengths in these two parts can be obtained in a linear approximation respectively as

$$\lambda_{\mathrm{MS1}} \sim \lambda_{\mathrm{JH}} \Lambda \quad \text{(in the lateral periodic diffusion field part)} \tag{16}$$

$$\lambda_{\mathrm{MS2}} \sim \lambda_{\mathrm{JH}} |(c^0 - c_{\mathrm{E}})/(c_\beta - c_\alpha)|^{-0.5}/\Lambda \quad \text{(in the 1D diffusion field part).} \tag{17}$$

At an eutectic or near-eutectic composition, there is a vanishing 1D diffusion field, and when λ_{MS1} first reaches a value comparable with 1λ as Λ increases, the $1\lambda O$ instability should first occur (primary $1\lambda O$) according to the criterion[3] pointed out by Karma. While at an off-eutectic composition, λ_{MS2} first ar-

rives at a value comparable with 2λ as Λ increases and it is the dominating instability wavelength, therefore the $2\lambda O$ instability should first arise (primary $2\lambda O$).

5. Conclusions

(i) A great number of instability modes observed in experiments are simulated in the eutectic alloy CBr_4–C_2Cl_6 under different conditions. There is a nice morphological similarity between the simulated patterns and experimental ones.

(ii) The stability diagrams of directionally solidified CBr_4–C_2Cl_6 by simulation are in good agreement with the numerical calculations and measurements. The formation of the primary instabilities is attributed to the destabilization of the solute boundary layer.

References

[1] Jackson K A and Hunt J D 1966 *Trans. TMS-AIME* **236** 1129

[2] Datye W and Langer J S 1981 *Phys. Rev.* B **24** 4155

[3] Karma A 1987 *Phys. Rev. Lett.* **59** 71

[4] Karma A and Sarkissian A 1996 *Mater. Trans.* A **27** 635

[5] Ginibre M, Akamatsu S and Faivre G 1997 *Phys. Rev.* E **56** 780

[6] Nestler B and Wheeler A A 2000 *Physica* D **138** 114

[7] Drolet F, Elder K R, Grant M and Kosterlitz J M 2000 *Phys. Rev.* E **61** 6705

[8] Apel M, Boettger B, Diepers H J and Steinbach I 2002 *J. Cryst. Growth* **237** 154

[9] Folch R and Plapp M 2003 *Phys. Rev.* E **68** 010602(R)

[10] Kim S G, Kim W T, Suzuki T and Ode M 2004 *J. Cryst. Growth* **261** 135

[11] Steinbach I and Pezzolla F 1999 *Physica* D **134** 385

[12] Mergy J, Faivre G, Guthmann C and Mellet R 1993 *J. Cryst. Growth* **134** 353

[13] Lee K 2004 *Analysis and Control of Microstructure* (University of Maryland) p103

[14] Zhu M F and Hong C P 2002 *Phys. Rev.* B **66** 155428

[15] Mullins W W and Sekerka R F 1964 *J. Appl. Phys.* **35** 444